Holographic laser Doppler imaging of pulsatile blood flow

Jeffrey Bencteux
Pierre Pagnoux
Thomas Kostas
Sam Bayat
Michael Atlan

Holographic laser Doppler imaging of pulsatile blood flow

Jeffrey Bencteux,[a] **Pierre Pagnoux,**[a] **Thomas Kostas,**[a] **Sam Bayat,**[b] **and Michael Atlan**[a,*]
[a]Centre National de la Recherche Scientifique (CNRS) UMR 7587, Institut Langevin, Fondation Pierre-Gilles de Gennes, Institut National de la Santé et de la Recherche Médicale (INSERM) U 979, UPMC, Université Paris 7, Ecole Supérieure de Physique et de Chimie Industrielles ESPCI ParisTech - 1 rue Jussieu, 75005 Paris, France
[b]Université de Picardie Jules Verne, INSERM U 1105, Paediatric Lung Function Laboratory, Amiens University Hospital, 80054 Amiens, France

Abstract. We report on wide-field imaging of pulsatile motion induced by blood flow using heterodyne holographic interferometry on the thumb of a healthy volunteer, in real time. Optical Doppler images were measured with green laser light by a frequency-shifted Mach-Zehnder interferometer in off-axis configuration. The recorded optical signal was linked to local instantaneous out-of-plane motion of the skin at velocities of a few hundreds of microns per second and compared to blood pulse monitored by plethysmoraphy during an occlusion-reperfusion experiment. © *2015 Society of Photo-Optical Instrumentation Engineers (SPIE)* [DOI: 10.1117/1.JBO.20.6.066006]

1 Introduction

One of the most commonly displayed clinical waveforms is the finger plethysmogram. It allows the noninvasive measurement of pulse wave amplitude, which reflects the changes in finger blood flow. It is usually recorded by a pressure sensor[1] or a pulse oximeter, which illuminates the skin and measures changes in optical absorption.[2–4] Optical plethysmography is widely available; its feasibility has even been demonstrated using mobile phones.[5,6] However, it does not provide a spatially resolved image. This limitation can be overcome by signal processing of regular video recordings in ambient light for time-dependent spatial and color fluctuations enhancement.[7–10] Other imaging approaches are designed to harness optical phase fluctuations of coherent laser light from the motion of body walls, either by single-point scanning detection,[11] direct image detection of temporal[12–14] and spatial speckle contrast,[15,16] or holographic interferometry.[17,18]

We report on narrowband laser Doppler imaging of superficial pulsatile motion of the thumb by heterodyne holographic interferometry with a camera refreshed at 60 Hz. A transient blood flow interruption experiment in a healthy volunteer is performed and compared to blood pulse monitoring. A major advantage of this system is that no physical contact with the studied tissue surface area is required. This could allow assessment of nonintact skin or mucous membranes or even the intraoperative study of tissues within the surgical field. Moreover, the lack of surface contact reduces the risk of infection transmission, which is a true concern with reusable contact-requiring biomedical equipment,[19] also avoiding the extra cost of disposable contact probes.

2 Experimental Setup

The experimental laser Doppler imaging scheme designed for this study is sketched in Fig. 1. The apparatus consists of a fibered Mach-Zehnder optical interferometer for off-axis[20] and frequency-shifting[21,22] holographic interferometry. The main optical radiation field is provided by a 150 mW, single-mode, fibered diode-pumped solid-state green laser (Cobolt Samba-TFB-150) at wavelength $\lambda = 532$ nm and optical frequency $\omega_L/(2\pi) = 5.6 \times 10^{14}$ Hz. The thumb is illuminated with ~10 mW of continuous optical power, over ~40 mm × 40 mm. In the reference channel, an optical local oscillator (LO) is formed by optical frequency shifting. Two acousto-optic modulators (Bragg cells, AA Opto Electronic), driven with phase-locked signals at ω_C and $\omega_C + \Delta\omega$, are used to shift the optical frequency of the laser beam from ω_L to $\omega_L + \Delta\omega$. The carrier frequency $\omega_C/(2\pi)$ is set to 200 MHz, at the peak response of the fibered acousto-optic modulators. The backscattered optical field E is mixed with the LO field E_{LO} with a nonpolarizing beam splitter cube. A Ximea MQ042MG-CM camera records interference patterns at a frame rate of $\tau_S^{-1} = \omega_S/(2\pi) = 60$ Hz. Each raw interferogram of 2048 × 2048 pixels, digitally acquired at time t is noted $I(t) = |E(t) + E_{LO}(t)|^2$. A small angular tilt ~1 deg between E and E_{LO} ensures off-axis recording. The sensor is set ~50 cm away from the object plane. A convergent lens of 50 mm focal length is present in the object channel, in order to widen the lateral field of view of the holographic detection to ~50 mm. The backscattered laser optical field $E(t) = \mathcal{E} \exp[i\omega_L t + i\phi(t)]$ undergoes a phase variation $\phi(t)$, as a consequence of out-of-plane motion of the illuminated tissue. It is mixed with the LO field from the reference channel $E_{LO}(t) = \mathcal{E}_{LO} \exp[i\omega_L t + i\Delta\omega t]$, which is tuned to a close-by intermediate frequency $\omega_L + \Delta\omega$. The quantities $\mathcal{E}$ and $\mathcal{E}_{LO}$ are complex constants and i is the imaginary unit. The magnitude of a given optical Doppler component is retrieved by frequency downconversion within the camera's temporal bandwidth, ensured by nonlinear detection of the field E by the array of square-law sensors of the camera, which respond linearly with the optical irradiance $I(t) = |E(t) + E_{LO}(t)|^2$. The squared
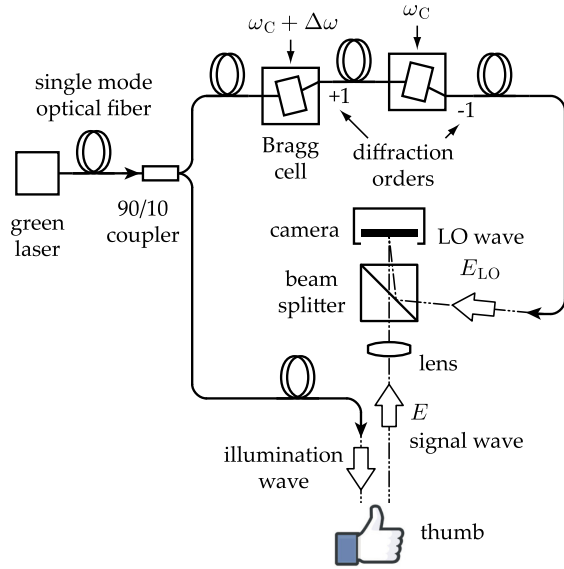
Fig. 1 Sketch of the fibered Mach-Zehnder heterodyne holographic interferometer. The main laser beam is split into two channels. In the object channel, the optical field E is backscattered by the skin. In the reference channel, the optical field E_{LO} is frequency-shifted by two Bragg cells by the quantity $\Delta\omega$. A standard camera records interferograms of the diffracted fields E and E_{LO}.

magnitude of the total field received, $E + E_{LO}$, has cross-terms oscillating at the difference frequency of the fields E and E_{LO}

$$I(t) = |\mathcal{E}|^2 + |\mathcal{E}_{LO}|^2 + H(t) + H^*(t), \tag{1}$$

where $H(t) = \mathcal{E}\mathcal{E}_{LO}^* \exp(i\phi - i\Delta\omega t)$ is the heterodyne interferometric contribution, and $*$ denotes the complex conjugate. This equation describes the temporal fluctuation of the recorded irradiance at a given pixel.

3 Signal Processing

Holographic image rendering, or spatial demodulation, is then performed onto each recorded interferogram I with a discrete Fresnel transform.[23] In off-axis recording configuration, the Fresnel transform separates spatially the four interferometric terms of the right-hand term of Eq. (1).[20,24] After spatial demodulation of each interferogram, the heterodyne signal $H(t)$ appears in the off-axis region of the hologram, processed as follows. First, the squared amplitude of the difference of two consecutive off-axis holograms is formed in order to cancel very low frequency noise contributions $S^2 = |H(t) - H(t - \tau_S)|^2$. Then, to cancel laser intensity fluctuations, a normalization factor $\langle S_0^2 \rangle = \langle |H_0(t) - H_0(t - \tau_S)|^2 \rangle$ is formed. The contribution H_0 is measured in a region of interest of the reconstructed hologram where the terms of Eq. (1) are not present,[25] and the brackets $\langle\,\rangle$ account for spatial averaging. In high heterodyne gain regime, i.e., when $|\mathcal{E}|^2 \ll |\mathcal{E}_{LO}|^2$, the quantity $\langle S_0^2 \rangle$ is dominated by shot-noise of the LO,[26,27] which scales up linearly with $|\mathcal{E}_{LO}|^2$. The averaged signal $\langle S^2 \rangle$ scales up linearly with $|\mathcal{E}|^2|\mathcal{E}_{LO}|^2$. Hence, the processed Doppler signal $\langle S^2 \rangle / \langle S_0^2 \rangle$ is a heterodyne measurement of the optical power (or irradiance) $|\mathcal{E}|^2$, which does not depend on the LO power.[28]

4 Narrowband Apparatus Response

Two-phase demodulation of interferograms recorded with a sampling frequency approximately equal to the reciprocal of
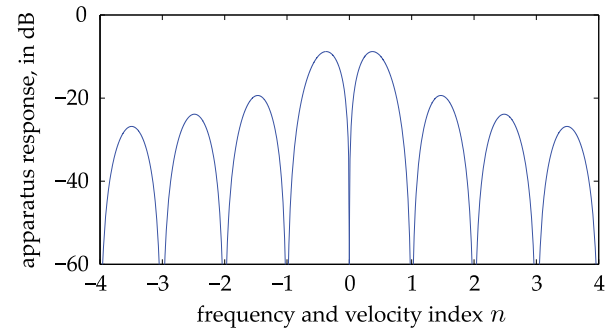
Fig. 2 Apparatus response [Eq. (2)], calculated for $\tau_S = \tau_E$, versus apparent (beating) frequency index $n = \omega/\omega_S$. The ticks of the horizontal axis correspond to the zeros of the response at integer values of the index n of the beating frequency $n\omega_S$ and the probed velocity $v_n = (\Delta\omega + n\omega_S)/(2k)$.

the exposure time ($\tau_S^{-1} \simeq \tau_E^{-1}$) results in a narrowband detection with an apparatus response plotted in Fig. 2. This response filters off optical contributions, which are not shifted in frequency, i.e., statically scattered light. For the backscattered field's irradiance $|\mathcal{E}|^2$, this response is[29,30]

$$B(\omega) = \frac{1}{\omega^2 \tau_E^2} \sin^2\left(\frac{\omega\tau_S}{2}\right) \sin^2\left(\frac{\omega\tau_E}{2}\right), \tag{2}$$

where ω is the apparent frequency recorded by the camera, as a result of heterodyne beating.

Let us assume that at the short time scale of the sampling process $t < \tau_S = 2\pi/\omega_S$, the local instant velocity is approximately constant; $v(t) \approx v(t - \tau_S) \approx v$. In other words, its magnitude v is identified to the time-averaged value of the instant velocity during τ_S, so we can simply write the local optical phase variation due to the transverse displacement of the skin as $\phi(t) = 2kvt = \omega t$, when the illumination and the scattered wave vectors are perpendicular to the skin's surface. The optical wave number is $k = 2\pi/\lambda \simeq 1.2 \times 10^7$ rad $\cdot$ s^{-1}, and $\omega = 2kv$. Now let us consider temporal variations of the instant velocity of norm $v(t)$ at long time scales $t > \tau_S$. The light reflected by the skin undergoes a local time-dependent Doppler shift
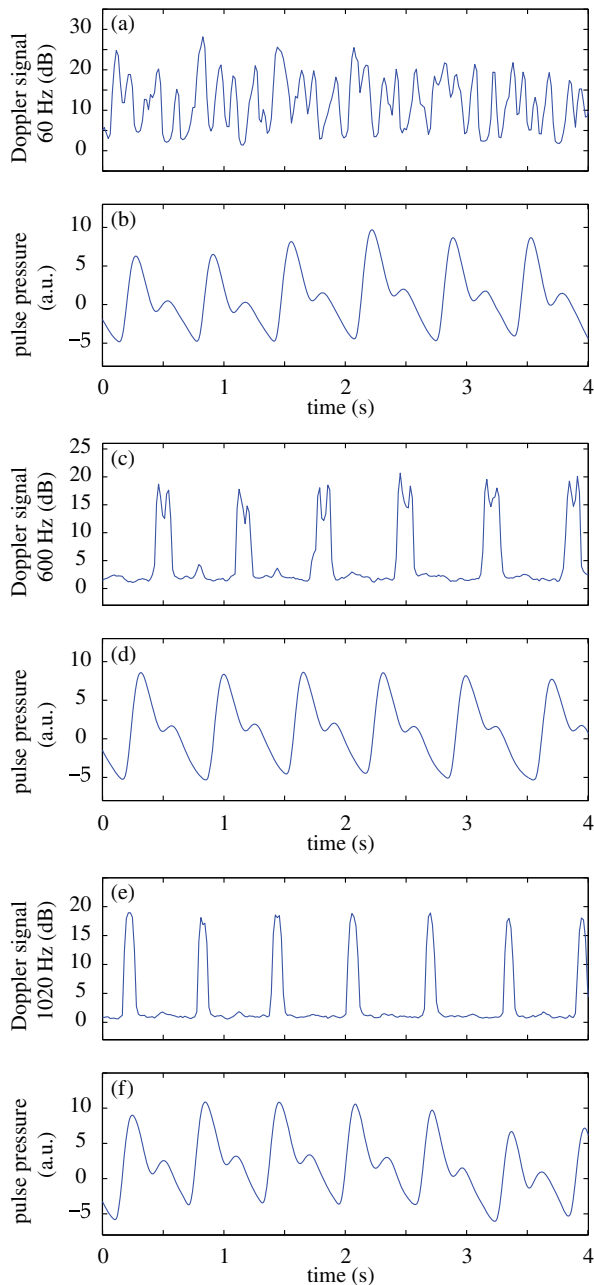
$$\omega(t) = 2kv(t). \tag{3}$$

To assess a given instant velocity v_0, the LO is detuned by $\Delta\omega = 2kv_0$. According to Eqs. (2) and (3), it results in the detection of Doppler-shifted light with a velocity-dependent efficiency $B[2k(v - v_0)]$. The range of probed velocities v within the two first lobes of the apparatus response B is

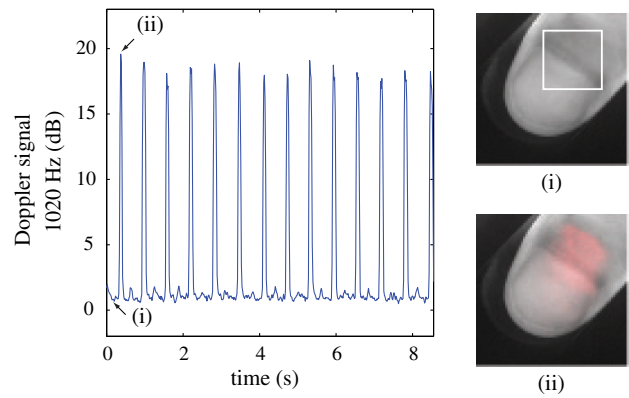$$[v_{-1}, v_{+1}] = \left[v_0 - \frac{\omega_S}{2k}, v_0 + \frac{\omega_S}{2k}\right]. \tag{4}$$

5 Experiment

An experiment on the fingers of healthy volunteers undergoing arterial occlusion provoked with a pressure cuff was conducted. All the subjects were coauthors of the study. Internal review board approval and the requirement for informed consent were waived for this observational study. The pressure cuff was placed around the right arm. The cuff bladder pressure was measured using a transducer (MLT0670, ADInstruments, Oxford, United Kingdom). The signal was amplified, digitized at 200 Hz using an analog/digital converter (Powerlab; ADI

Fig. 4 Optical Doppler signal, acquired for a detuning frequency $\Delta\omega/(2\pi) = 1020$ Hz, averaged in the region of interest depicted in (i), versus time. Composite images of the corresponding signal at (i) low and (ii) high signal level. Red color indicates signal presence. The whole sequence is reported in Video 1 (MOV, 2.45 MB) [DOI: http://dx.doi.org/10.1117/1.JBO.20.6.066006.1].
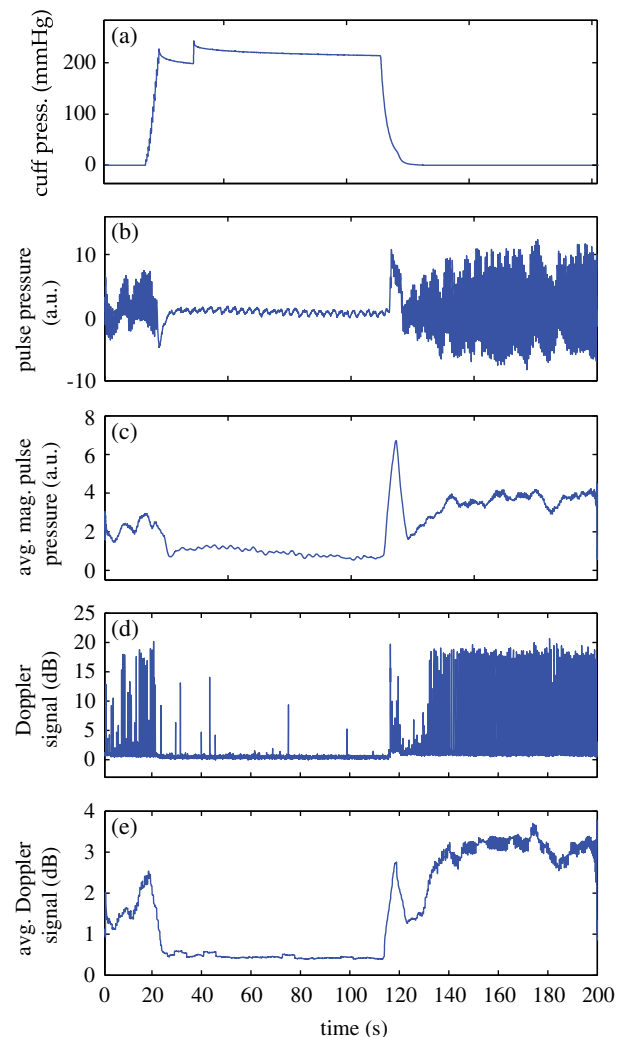

Fig. 3 Doppler signal [(a), (c), and (e)], averaged in the central part of the image of the thumb (Fig. 4), and concurrent blood volume signal [(b), (d), and (f)], versus time. Detuning frequencies: (a) $\Delta\omega/(2\pi) =$ 60 Hz, (c) $\Delta\omega/(2\pi) = 600$ Hz, and (e) $\Delta\omega/(2\pi) = 1020$ Hz. The synchronization accuracy of holographic and standard blood volume measurements is on the order of ±0.5 s. a.u., arbitrary units.

Instruments), and recorded on a computer. The arterial pulse wave was monitored using a piezo-electric pulse transducer (TN1012/ST, ADInstruments) placed on the index of the imaged hand. The signal was recorded at 200 Hz. The thumb was illuminated by the green laser beam. A comfortable support for the forearm was used to avoid stray motion. A preliminary experiment was performed to monitor the Doppler response at three different detuning frequencies $\Delta\omega/(2\pi)$: 60, 600, and 1020 Hz; choosing a detuning frequency that is an integer number of times the sampling frequency is not mandatory, but has the advantage of canceling efficiently statically backscattered light, according

Fig. 5 Time traces of indicators monitored during a hypoperfusion experiment. (a) Cuff pressure, plethysmogram [(b) raw data, (c) 5 s time-average of the magnitude], holographic laser Doppler signal recorded at 1020 Hz and averaged spatially in the nail area [(d) raw data, (e) 5 s time-average]. A time-lapse sequence of the composite Doppler image of the thumb is reported in Video 2 (MOV, 1.32 MB) [DOI: http://dx.doi.org/10.1117/1.JBO.20.6.066006.2].

to the apparatus response (Fig. 2). These frequencies correspond to probed velocities of 16, 160, and 271 μm · s^{-1}, respectively. Figure 3 shows plots over time of pulse waveforms (plethysmograms) and holographic Doppler signal $10 \log_{10}(\langle S^2 \rangle / \langle S_0^2 \rangle)$ (in dB) averaged in a region of interest, placed on the central part of the image of the thumb. At very low frequency detunings ($\lesssim 100$ Hz), motion artifacts prevented the measurement of pulsatile motion. When the frequency was set to $\Delta\omega/(2\pi) = 1020$ Hz, which corresponded to a measurement range of instant velocities $[v_{-1}, v_{+1}] = [255 \, \mu\text{m} \cdot \text{s}^{-1}, 287 \, \mu\text{m} \cdot \text{s}^{-1}]$, centered at $v_0 = \Delta\omega/(2k) = 271 \, \mu\text{m} \cdot \text{s}^{-1}$ [Eq. (4)], the Doppler signal appeared to be less prone to motion artifacts. The Doppler signal at 1020 Hz recorded over ~8 s, and composite images of the regionalized Doppler response (represented in red) are displayed in Fig. 4 and in Video 1. This value of the frequency shift was chosen for the blood flow interruption experiment, reported in Fig. 5. The cuff pressure and four indicators were monitored: pulse wave, 5 s-averaged pulse wave magnitude, Doppler signal, and 5 s-averaged Doppler signal. Blood flow to the forearm was occluded by increasing the cuff pressure to ~200 mm Hg during an ~90 s time interval. During occlusion, both recorded signals dropped. Short spikes due to motion artifacts were observed on the Doppler signal; they were more pronounced at a lower Doppler frequency. On releasing the cuff pressure, a transient increase of both the pulse volume and the Doppler signal is observed as expected, due to postocclusive hyperemia. A time-lapse sequence of the composite Doppler image of the thumb during the occlusion-reperfusion experiment is reported in Video 2. A limitation of holographic Doppler imaging of pulsatile blood flow with visible laser light is its sensitivity to low velocities, which enables motion artifacts to prevent the measurement of pulsatile motion, and requirement for stabilization of the monitored tissue. This issue might be alleviated with infrared light.

6 Conclusion

We demonstrated wide-field imaging and monitoring of pulsatile motion of the thumb of a healthy volunteer. Narrowband optical Doppler video imaging in real time was performed with an off-axis and frequency-shifting holographic interferometer. Numerical image rendering was performed by discrete Fresnel transformation and two-phase temporal demodulation at a 60 Hz frame rate. The measured contrast was linked to the instant velocity of out-of-plane motion, of the order of a few hundreds of microns per second. Robust noncontact motion monitoring was achieved. This was illustrated by an occlusion-reperfusion experiment, in which the proposed detection scheme was compared to plethysmography.

References

1. W. F. Ganong and K. E. Barrett, *Review of Medical Physiology*, Volume 22, McGraw-Hill, New York (2005).

2. A. B. Hertzman and C. R. Spealman, "Observations on the finger volume pulse recorded photoelectrically," *Am. J. Physiol.* **119**, 334–335 (1937).
3. J. Allen, "Photoplethysmography and its application in clinical physiological measurement," *Physiol. Meas.* **28**(3), R1 (2007).
4. A. A. Alian and K. H. Shelley, "Photoplethysmography," *Best Pract. Res. Clin. Anaesthesiol.* (2014).
5. E. Jonathan and M. Leahy, "Investigating a smartphone imaging unit for photoplethysmography," *Physiol. Meas.* **31**(11), N79 (2010).
6. C. Scully et al., "Physiological parameter monitoring from optical recordings with a mobile phone," *IEEE Trans. Biomed. Eng.* **59**(2), 303–306 (2012).
7. C. Takano and Y. Ohta, "Heart rate measurement based on a time-lapse image," *Med. Eng. Phys.* **29**(8), 853–857 (2007).
8. L. Scalise et al., "Heart rate measurement in neonatal patients using a webcamera," in *IEEE Int. Symp. on Medical Measurements and Applications*, pp. 1–4, IEEE (2012).
9. H.-Y. Wu et al., "Eulerian video magnification for revealing subtle changes in the world," *ACM Trans. Graph.* **31**(4), 65 (2012).
10. G. Balakrishnan, F. Durand, and J. Guttag, "Detecting pulse from head motions in video," in *IEEE Conf. on Computer Vision and Pattern Recognition*, pp. 3430–3437, IEEE (2013).
11. T. J. H. Essex and P. O. Byrne, "A laser Doppler scanner for imaging blood flow in skin," *J. Biomed. Eng.* **13**(3), 189–194 (1991).
12. M. Draijer et al., "Twente optical perfusion camera: system overview and performance for video rate laser Doppler perfusion imaging," *Opt. Express* **17**(5), 3211–3225 (2009).
13. M. Leutenegger et al., "Real-time full field laser Doppler imaging," *Biomed. Opt. Express* **2**(6), 1470–1477 (2011).
14. A. A. Kamshilin et al., "Variability of microcirculation detected by blood pulsation imaging," *PloS One* **8**(2), e57117 (2013).
15. D. A. Boas and A. K. Dunn, "Laser speckle contrast imaging in biomedical optics," *J. Biomed. Opt.* **15**(1), 011109 (2010).
16. A. Humeau-Heurtier et al., "Skin perfusion evaluation between laser speckle contrast imaging and laser Doppler flowmetry," *Opt. Commun.* **291**, 482–487 (2013).
17. M. Leclercq et al., "Evaluation of surface acoustic waves on the human skin using quasi-time-averaged digital Fresnel holograms," *Appl. Opt.* **52**, A136–A146 (2013).
18. I. Dobrev et al., "Optimization of a lensless digital holographic otoscope system for transient measurements of the human tympanic membrane," *Exp. Mech.* 1–12 (2014).
19. A. B. Hertzman, "Photoelectric Plethysmography of the Fingers and Toes in Man," *Exp Biol Med (Maywood)* **37**, 529–534 (1937).
20. E. N. Leith and J. Upatnieks, "Reconstructed wavefronts and communication theory," *JOSA* **52**(10), 1123–1128 (1962).
21. C. C. Aleksoff, "Time average holography extended," *Appl. Phys. Lett.* **14**, 23 (1969).
22. A. Macovski, "Efficient holography using temporal modulation," *Appl. Phys. Lett.* **14**(5), 166–168 (1969).
23. J. W. Goodman and R. W. Lawrence, "Digital image formation from electronically detected holograms," *Appl. Phys. Lett.* **11**(3), 77–79 (1967).
24. E. Cuche, P. Marquet, and C. Depeursinge, "Spatial filtering for zero-order and twin-image elimination in digital off-axis holography," *Appl. Opt.* **39**(23), 4070 (2000).
25. M. Atlan and M. Gross, "Laser Doppler imaging, revisited," *Rev. Sci. Instrum.* **77**(11), 116103 (2006).
26. M. Gross and M. Atlan, "Digital holography with ultimate sensitivity," *Opt. Lett.* **32**(8), 909–911 (2007).
27. M. Lesaffre, N. Verrier, and M. Gross, "Noise and signal scaling factors in digital holography in weak illumination: relationship with shot noise," *Appl. Opt.* **52**(1), A81–A91 (2013).
28. C. Magnain et al., "Holographic laser Doppler imaging of microvascular blood flow," *JOSAA* (2014).
29. M. Atlan et al., "Parallel heterodyne detection of dynamic light-scattering spectra from gold nanoparticles diffusing in viscous fluids," *Opt. Lett.* **35**(5), 787–789 (2010).
30. N. Verrier, D. Alexandre, and M. Gross, "Laser Doppler holographic microscopy in transmission: application to fish embryo imaging," *Opt. Express* **22**(8), 9368–9379 (2014).

Biographies of the authors are not available.